DEFORMATION OF THE ENERGY SPECTRUM FROM A ^{99M}TC SOURCE WITH ITS DEPTH

V. Breton, D. Lazaro, L. Méritet, J. Berthot, G. Montarou LPC, Clermont-Ferrand, France
J. Maublant, C. Thouly CJP, Clermont-Ferrand, France

Abstract

Planar scintimammography with ^{99m}Tc-Sestamibi is a sensitive, specific and non invasive method used in complement to X-ray mammography for breast cancer diagnosis. Studies [1] have shown how scatter correction might improve lesion detection and quantitation of tumor-to-normal breast tissue activity ratio. Among the strategies used to compute this correction, some are based on the analysis of the energy spectrum of photons [2].
In a similar approach, this paper presents experimental and Monte-Carlo results on the deformation of the energy spectrum in correlation with the depth of the source. It focuses on the exploitation of the deformation of the energy spectrum to compute the depth of a tumor.

1 MOTIVATION

Planar scintimammography has not yet been proven to be overthrown by SPECT. Its specifity of about 87-89 % and sensitivity of about 92 % [3] decreases to 50 % when considering small lesions. An approach to improve the detection of small lesions is to try to better exploit ALL the information collected in planar scintigraphy. Indeed, the part of the energy spectrum used for image reconstruction is the one defined by the acquisition energy window. Typically centred on the emission energy of the isotope, its width defined as a percentage of this energy, usually 20% (e.g. 126-154 keV for ^{99m}Tc), can be shrunk to reduce scatter contamination. Several groups are now working on studying the effects of Compton scattering on image contrast and lesion detection [4,5,6,7]. Many scatter correction techniques have been studied and developed during last years [8,9,10]. Among the different strategies successfully applied to compute scatter corrections, the so-called FA [2], Factor Analysis-based scatter correction, is based on an analysis of the energy spectrum of the photons down to 50 keV.
Indeed, for a source located at a given depth in the body, the probability for a photon emitted by the source to undergo Compton scattering before reaching the camera grows with the depth of tissue to cross. Two effects are therefore observed :

- the number of photons reaching the camera without undergoing Compton scattering decreases when the depth increases. The photoelectric peak is therefore depleted with respect to the Compton peak. This well known effect has already been studied for instance in [4,6].
- as the average number of Compton scatters increases with the depth, the average energy in the Compton distribution should decrease. The shape of the distribution is thus expected to be modified. Ljunberg [11] and Floyd [7] have already noticed that the shape of scatter projections changes with depth source, becoming more flattened as the source is imaged at greater depths.

The goal of this paper is to describe the impact of these two effects on the energy spectrum and to propose estimators quantifying its deformation. These estimators could be used to evaluate a source depth in planar scintimammography. Our study was done in two steps :

- in a first step, we investigated experimentally the magnitude of the energy spectrum deformation of 1mCi sources using a gamma camera Sopha-Medical DSX. at the Centre Anticancereux Jean Perrin in Clermont-Ferrand. The sources were put inside phantoms of variable thickness. For each set-up, the images were collected simultaneously in 4 energy windows.
- In a second step, we developed a very detailed Monte-Carlo simulation of the gamma-camera using GEANT in order to reproduce the deformation observed. Once the simulation was optimised, we studied the role of the collimator in the deformation of the energy spectrum.

2 DEFORMATION OF THE ENERGY SPECTRUM : EXPERIMENTAL RESULTS

The experimental protocol consists in the simultaneous detection of the photons emitted by a 1mCi ($3.7.10^{10}$ Bq) ^{99m}Tc source in 4 energy windows : 126-154 keV, 94-126 keV, 66-94 keV and 46-66 keV. In the following, we will call them respectively Window 1 (W_1), Window 2 (W_2), Window 3 (W_3) and Window 4 (W_4). The source is a $1cm^3$ cube located 10 cm away from the camera collimator front face. Between the source and the camera, 1cm-thick layers of plexiglass were introduced (figure 1) and 128×128

pixels images were acquired in the four energy windows for 0, 1, 2, 3, 4, 5 and 6 layers. Pixel size was set to 0.5 cm. The acquisition times were set to 60 s and 180 s. The acquisition times were different in order to prevent pixel overflow during acquisition in photopeak window W_1 and to allow to collect thousands of counts in the Compton peak for each set-up. Figure 1 shows also the images collected simultaneously of the source in the 4 energy windows for 4 layers of plexiglass and 60s acquisition time. The four images have the same relative grey scales. As expected, going from window W_1 (126-154 keV) to window W_4 (46-66 keV), the image of the source has less and less contrast. However, the deformation of the image from W_1 to W_4 carries information on the amount of material crossed by the photons to reach the camera.

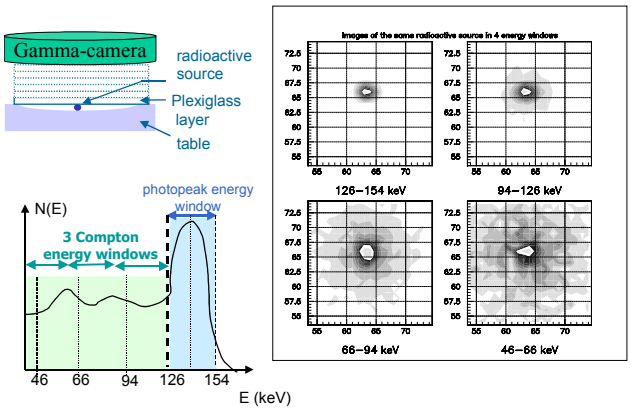

Figure 1: experimental setup. Images of the same ^{99m}Tc radioactive source taken simultaneously in 4 energy windows.

2.1 Correlation between the source depth and its images first moments

In each energy window, the images were analysed by looking at the first moment M1(n), number of counts integrated on the (2n+1)×(2n+1) matrix centered on the hottest pixel. The definition of the hottest pixel is unambiguously related to the position of the source for the image taken in the energy window W_1 centred on the photoelectric peak. We used this pixel as the centre of reference for the computation of first order moments for all images.

Figure 2 shows M1(n) for n varying from 0 (only the central pixel) to 20 (integration on a 41×41 pixels square). Matrix were obtained for a 60 s acquisition time. The different symbols correspond to different layers of plexiglass between the source and the camera. Error bars are smaller than the symbols. The two plots corresponding to windows W_1 and W_4 show opposite trends when the plexiglass layer increases. The number of events in the W_4 (46-66 keV) window increases while the number of events in the W_1 (126-154 keV) window decreases. This effect was expected as the plexiglass layer absorbs and scatters photons: these two processes contribute to depopulate the photoelectric peak. On the other hand, scattering and absorption have opposite impact on the Compton peak: scattering contributes to populate the Compton distribution while absorption depopulates it.

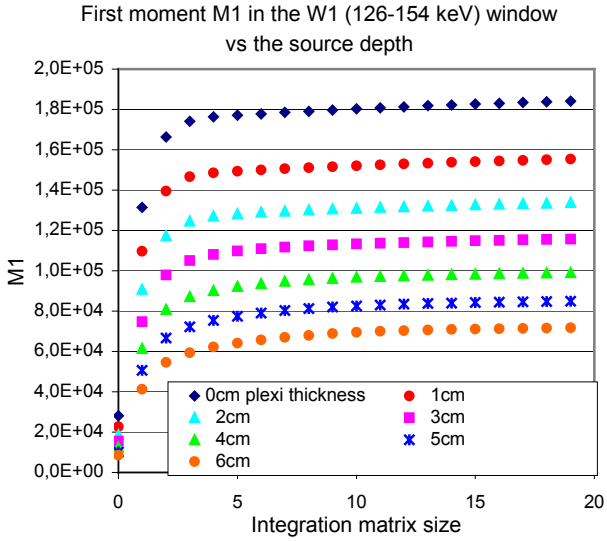

Figure 2 : first moment M1 of the source spot integrated on a matrix of (2n+1)x(2n+1) pixels in W_1. The different symbols correspond to different layers of plexiglass between the source and the camera.

A way to quantify the deformation between the images in the W_1 and W_4 windows is to compute the ratio of the first moments M1(n). Such ratio is independent of the source activity. Figure 3 shows this ratio $M_1^{W4}(n)/M_1^{W1}(n)$ of the first moments M1(n) in windows W_1 (126-154 keV) and W_4(46-66 keV) for n varying from 1 to 20 pixels. Error bars are smaller than the symbols.

A very interesting feature is the fact that the ratio $M_1^{W4}(n)/M_1^{W1}(n)$ is significantly correlated to the plexiglass thickness already for small matrices (n=2,3,4). This means that the deformation of the images from W_1 to W_4 carries information on the source depth even if one looks only at the vicinity of the hottest spot. This could become important when considering distributed sources.

2.2 Deformation of the Compton peak

Another consequence of multiple scattering inside the plexiglass layer is the deformation of the Compton distribution. One expects a shift of the Compton events to lower energy. Indeed, the contribution of multiply scattered photons increases as the depth of the source in the scattering medium increases.

This effect can be quantified by studying the ratio $M_1^{W4}(n)/(M_1^{W2}(n)+ M_1^{W3}(n)+M_1^{W4}(n))$ of the number

of events in the W_4 window (46-66 keV) to the number of events in the total Compton window (46-126 keV).

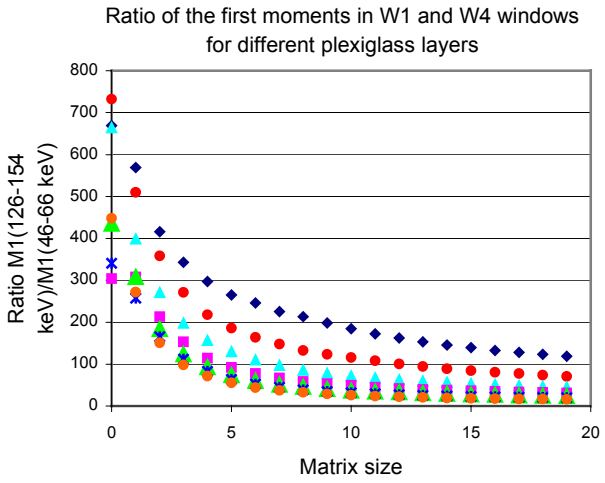

Figure 3 : ratio of the first moment M1 in the energy window W_1 (126-154 keV) to M1 in the energy window W_4 (46-66 keV).

Figure 4 shows this ratio for n varying from 1 to 20 pixels and different layers of plexiglass. Error bars are smaller than the symbols. The fraction of Compton events in W_4 is clearly correlated to the amount of plexiglass crossed.

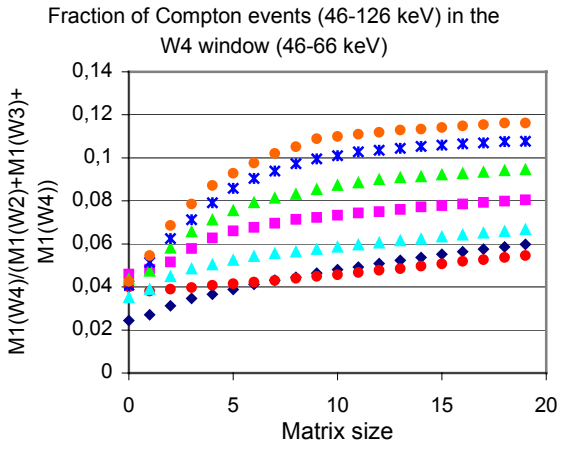

Figure 4 : ratio of the first moment M1 in the energy window W_4 (46-66 keV) to M1 in the energy window W (46-126 keV).

2.3 Summary of the experimental results

A deformation of the energy spectrum has been observed when detecting photons coming from a ^{99m}Tc source after crossing plexiglass of variable thickness. We identified two quantities which are independent of the source activity and which are correlated to the amount of plexiglass between the source and the camera :

- the ratio M_1^{W4}/M_1^{W1} of the first moments M1 in windows W_1 (126-154 keV) and W4 (46-66 keV). It also appeared that the ratio M_1^{W4}/M_1^{W1} is the most sensitive quantity to distinguish ratios for different source depths if we consider same size matrix. It remains the most sensitive even if we take into account the vicinity of the source.
- the ratio $M_1^{W4}/(M_1^{W2}+ M_1^{W3}+M_1^{W4})$ of the number of events in the W_4 window (46-66 keV) to the number of events in the Compton peak (46-126 keV)

These results were obtained with a Sopha-Medical DSX gamma camera routinely used at Centre Jean Perrin. They might open the perspective of using the Compton events to measure the depth of a source in planar scintigraphy.

The next step of this study was to try to reproduce the effects observed experimentally with a Monte-Carlo simulation.

3 MONTE-CARLO SIMULATION WITH GEANT

Many Monte Carlo programs are used in the field of nuclear medicine. Zaidi [12] proposed a detailed overview of the different available simulation codes. Among these codes one find the GEANT simulation package. For more than 2 decades, the subatomic physics community around the world has been using the Monte Carlo code GEANT to describe the interaction of ionising particles with matter. The GEANT code was developed at CERN to deal with the increasing scale and complexity of the high energy physics experiments. The interest of using GEANT to simulate gamma-cameras is threefold :

- All the physics processes involved from the emission of the radioisotope to the creation of the image in the gamma-camera are described in GEANT or can be added.
- The code is highly reliable because it is used extensively around the world.
- The code is a standard in high energy physics and therefore there is abundant documentation and many experts.

Two versions of GEANT are available :

- GEANT version 3 [13] was written in Fortran by a team at CERN as a complete update from previous versions in the 90's. Concerning medical imaging applications, electromagnetic processes are simulated down to 10 keV,
- GEANT version 4.2 is a completely new code developed within an international collaboration of about 100 scientists participating in more than 10 experiments in Europe, Russia, Japan, Canada and the United States. To extend its use toward medical physics and space physics, very

low energy electromagnetic processes down to hundred electron-volts are included. Written in object-oriented language, the GEANT4 source code is freely available [14]. The code provides the transparency of the physics implementation. It can also be interfaced with many graphical systems, which offers a graphical representation of the setup and of the particle trajectories and makes the debugging easier.

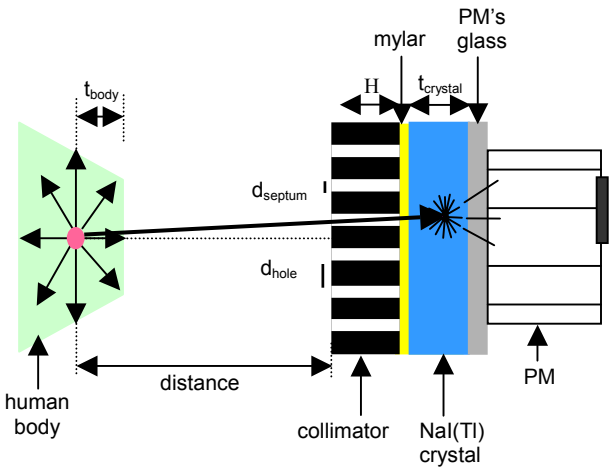

Figure 5: The different elements of the geometry.

We are going to describe the different parts of the simulation code. Figure 5 shows the different elements of the complete geometry available under GEANT3: source(s), body, collimator, crystal and photomultiplier tubes. More details can be found in [15]. The simulation code with GEANT4 is under development and concerns only the setup source-collimator-crystal.

3.1 Sources

The point-like sources are located inside the breast. Their number, size, shape and position are parameters adjustable at execution time. We considered only ^{99m}Tc isotropic sources emitting 140 keV photons.

3.2 Body

Body was simulated by a trapezoid of variable thickness. Breast tissue atomic composition was taken from NIST web site [16]. In the body, photons emitted from the sources undergo Compton scattering and photoelectric effect. Rayleigh scattering was neglected.

3.3 Collimator

Among the gamma cameras on the market, many options for the geometry of the collimators are considered depending upon the specific needs. For the purpose of validating the simulation, we considered 2 widely used configurations : parallel-hole and pin-hole geometry. For parallel hole collimators, we considered hexagonal cells placed in a fly's eye configuration separated by thin foils. Among the heavy materials used for collimators, we chose lead.
The hole diameter, the septa thickness and the collimator thickness as well as its material are free parameters of the simulation.

3.4 Crystal

One of the hardest issues for the Monte-Carlo simulation of gamma cameras concerns the treatment of optical photons generated by scintillation in the doped NaI(Tl) crystal. Indeed, about 40000 optical photons per MeV of energy are generated. Each photon must be followed in its travel inside the crystal to the photomultipliers entrance window. GEANT321 allows a reliable description of optical photons transport, reflection and refraction. It has however no treatment of scintillation. We therefore added our own generation of optical photons : when GEANT stops tracking photons and electrons inside the crystal because they fell below the energy threshold (≈ 10 keV), 3eV optical photons are generated isotropically at stopping point : 40000 optical photons per MeV incident energy are then tracked by GEANT3.

3.5 Light collection

Light collection is probably the weakest point of our simulation because we did not enter into the details of describing the electronic shower in the photomultipliers. We considered absorbing surfaces around the crystal and for the crystal entrance surface, and a diffusing surface for the crystal exit window. Indeed, it has been shown [17] that a such surface treatment limits image distorsion.
In this work, the number of photons collected by the PM's was adjusted varying the quantum efficiency. Photomultipliers output was calibrated on the photoelectric peak.
We first checked the validity of the simulation by comparing the collimator performances to analytical formulas based on geometrical considerations [18]. The energy resolution of the camera was tuned by varying the crystal thickness and the quantum efficiency of the photomultipliers. The sensitivity of the crystal was compared to experimental values from NIST.

3.6 Comparison of Geant3 and Geant4 results

Collimator performances

Collimator performances are usually expressed in terms of spatial resolution and sensitivity. Spatial resolution is defined as the FWHM of the spatial distribution and the sensitivity is defined as the ratio of number of photons passing through the collimator to the number of incident photons.

For the simulation, the source is placed at a variable distance, noted d, from the collimator front face and emits 500 000 photons isotropically. Two

configurations of collimators were simulated: a pin-hole collimator and a parallel-hole collimator. Three geometries were investigated for the parallel-hole collimator:

- geometry n°1: hole diameter = 1,5 mm; septa thickness = 0,2 mm,
- geometry n°2: hole diameter = 1,9 mm; septa thickness = 0,5 mm,
- geometry n°3: hole diameter = 2,5 mm; septa thickness = 0,3 mm.

The hole diameter for the pin-hole collimator was set to 4,0 mm.

Table 1 presents results of the simulations performed with GEANT3 and GEANT4 and the values obtained by the analytical formulas for a distance between the source and the collimator front face of 10 cm.

Table 2 presents the same results for the collimator n°2 and d varying between 2 cm and 20 cm. Table 3 concerns the pin-hole collimator.

Table 1 : theoretical and simulated values of spatial resolutions and sensitivities for a distance of 10 cm between the source and the collimator.

Collimator type	R_{ANAL} (mm)	R_{SIMU} (mm)	S_{ANAL} (10^{-2} %)	S_{SIMU} (10^{-2} %)
Parallel n°1	6.67	G3: 6.0 G4: 6.4	1.41	G3: 1.34 G4: 1.42
Parallel n°2	8.45	G3: 8.3 G4: 8.4	1.82	G3: 1.65 G4: 1.83
Parallel n°3	11.1	G3: 12.0 G4: 10.0	4.01	G3: 3.84 G4: 4.02
Pin-hole	5.0	G3: 5.9 G4: 5.8	1.00	G3: 0.85 G4: 0.82

Table 2 : theoretical and simulated values of spatial resolutions and sensitivities for parallel-hole collimator n°2 for varying distance between the source and the collimator.

Distance d (cm)	R_{ANAL} (mm)	R_{SIMU} (mm)	S_{ANAL} (10^{-2} %)	S_{SIMU} (10^{-2} %)
2	3.25	G3: 2.5 G4: 2.2	1.82	G3: 1.71 G4: 1.81
5	5.20	G3: 4.8 G4: 4.6	1.82	G3: 1.68 G4: 1.85
10	8.45	G3: 8.3 G4: 8.4	1.82	G3: 1.65 G4: 1.83
20	14.9	G3: 14.5 G4: 14.2	1.82	G3: 0.71 G4: 1.82

Table 3 : theoretical and simulated values of spatial resolutions and sensitivities for pin-hole collimator for varying distance between the source and the collimator.

Distance d (cm)	R_{ANAL} (mm)	R_{SIMU} (mm)	S_{ANAL} (10^{-2} %)	S_{SIMU} (10^{-2} %)
2	10.0	G3: 10.99 G4: 10.25	19	G3: 25 G4: 18
5	7.0	G3: 7.37 G4: 7.07	3.3	G3: 4 G4: 3.2
10	5.0	G3: 5.97 G4: 5.82	0.85	G3: 1 G4: 0.82
20	4.6	G3: 5.54 G4: 5.38	0.21	G3: 0.25 G4: 0.21

It clearly appears that GEANT4 better reproduces sensitivity values than GEANT3. The results for spatial resolution are more ambiguous: the values obtained with GEANT4 are better when considering the pin-hole collimator but there is no evident improvement for the parallel-hole collimator.

Crystal sensitivity

The sensitivity of the crystal is defined as the ratio of the number of photons stopped in the crystal by a photoelectric effect to the incident photon number. The sensitivity was evaluated for different NaI(Tl) crystal thicknesses with the help of GEANT3 and GEANT4. The GEANT4 simulations were performed for the standard electromagnetic processes and the low-energy electromagnetic processes in order to achieve a complete comparison between GEANT3, GEANT4 and experimental values taken from NIST.

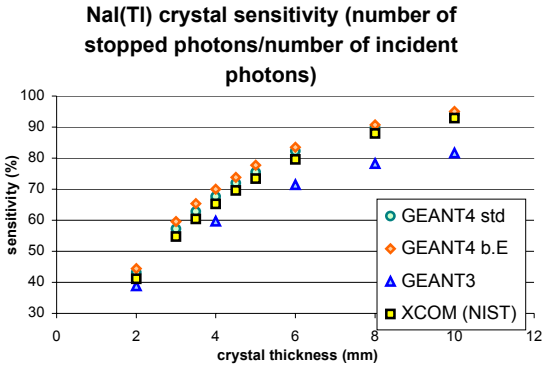

Figure 6: sensitivity of the NaI(Tl) crystal: comparison of simulation data obtained from GEANT3, GEANT4 standard, GEANT4 low-energy with NIST values.

GEANT3 curve shows an underestimation of photo-absorption cross sections of about 10 % whereas GEANT4 cross sections are very close to NIST values. The effect seems to become more and more important with the crystal thickness.

3.7 Deformation of the energy spectrum : Monte-Carlo result

Figure 7 shows the ratio $M_1^{W1}/(M_1^{W2}+ M_1^{W3}+M_1^{W4})$ of the number of events in the W1 window (126-154 keV) to the number of events in the 3 Compton windows (46-126 keV), computed at n=20, i.e. for a 41x41 pixels matrix, as a function of the plexiglass thickness, 0 to 6 cm, for 5 set of points :

- black squares correspond to the experimental data from Centre Jean Perrin
- black dots and white triangles are GEANT3 results respectively with and without treatment of optical photons with a parallel collimator (hole diameter: 3mm; septum thickness: 0.3mm; height: 30mm)

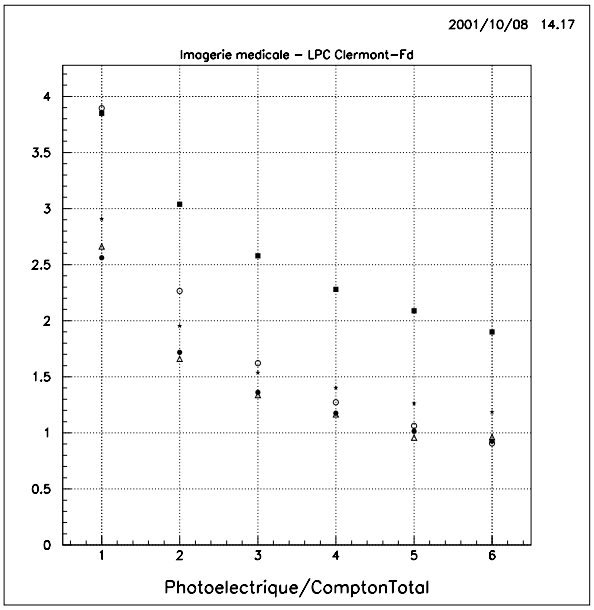

Figure 7: ratio $M_1^{W1}/(M_1^{W2}+ M_1^{W3}+M_1^{W4})$ of the number of events in the W1 window (126-154 keV) to the number of events in the 3 Compton windows (46-126 keV).

- white dots are GEANT3 results without collimator.
- stars are GEANT4 (low-energy package) with the same parallel collimator as the ones used with GEANT3 simulation.

The simulation shows the same behaviour as the experimental data, although the simulation underestimates the ratio compared to the data. Results with and without treatment of optical photons are very close. The correlation between the ratio and the plexiglass thickness remains significant when there is no collimator in front of the gamma camera.

4 CONCLUSION

We have presented in this paper the results of a comparative study of experimental data with Monte Carlo simulation regarding the shape of the energy spectrum of a ^{99m}Tc source in relation to the source depth. We observe experimentally a significant deformation of the energy spectrum correlated to the source depth. This deformation can be reproduced qualitatively by Geant3 and Geant4 simulations. A more detailed study will be now necessary to know how accurate is such a method on the determination of the source depth, in particular in the case of extended sources. Furthermore, the difference between experimental and simulation results has to be investigated.

5 BIBLIOGRAPHY

[1] I. Buvat et al, Impact of Scatter Correction in Planar Scintimammography: A Phantom Study, J. Nucl. Med. **39**, 1590-1596 (1998)

[2] I. Buvat et al, Comparative Assessment of nine scatter correction methods based on spectral analysis using Monte-Carlo simulations, J. Nucl. Med. **36**, 1476-1488 (1995)

[3] I. Khalkhali et al., Radiology, vol. **196**, no.2, 421-426 (1997)

[4] C. E. Floyd et al., Scatter detection in SPECT imaging: dependence on source depth, energy and energy window, Phys. Med. Biol. **33**, no. 9, 1075-1081 (1988)

[5] S. H. Manglos et al., Experimentally measured scatter fractions and energy spectra as a test of Monte Carlo simulations, Phys. Med. Biol. **32**, no. 3, 335-343 (1987)

[6] A. Kojima et al., Effect of energy resolution on scatter fraction in scintigraphic imaging: Monte Carlo study, Med. Phys. **20**, no. 4, 1107-1113 (1993)

[7] C. E. Floyd et al., Energy and spatial distribution of multiple order Compton scatter in SPECT: a Monte Carlo investigation, Phys. Med. Biol. **29**, no. 10, 1217-1230 (1984)

[8] R. J. Jaszczak et al., Scatter compensation techniques for SPECT, IEEE Tr. Nucl. Sci. **32**, 786-793 (1985)

[9] M. A. King et al., A dual-photopeak window method for scatter correction, J. Nucl. Med. **33**, 605-612 (1992)

[10] K. Ogawa et al., Simulation study of triple-energy-window scatter correction in combined Tl-201, Tc-99m SPECT, Ann. Nucl. Med. **8**, 277-281 (1994)

[11] M. Ljunberg et al., A Monte Carlo program for the simulation of scintillation camera characteristics, Computer Meth. and Prog. In Biomed. **29**, 257-272 (1989)

[12] H. Zaidi, Relevance of accurate Monte Carlo modeling in nuclear medical imaging, Med. Phys. **26**, no.4, 574-608 (1999)

[13] GEANT3, Detector description and simulation tool, Application Software Group, CERN Geneva, Switzerland, 1993

[14] GEANT4 web site : wwwinfo.cern.ch/asd/geant4/geant4.html

[15] J. Berthot et al, Monte-Carlo simulation of gamma-cameras using GEANT, proceedings of IEEE Medical Imaging Conference, Lyon 2000

[16] NIST web site: http://www.physics.nist.gov/PhysRefData

[17] C.E. Ordonez et al., Simulation of imaging with sodium iodide crystals and position-sensitive photomultiplier tubes, IEEE Tr. Nucl. Sci. **41**, no. 4, 1510-1515 (1994)
[18] H. O. Anger, Scintillation camera with multichannel collimators, J. Nucl. Med. **5**, 515-531 (1964)